from small to arbitrary injection levels. The theoretical approach differs from that of Goedbloed and Vlaardingerbroek [6] in that a phenomenological model of the active device has been chosen which considerably simplifies the mathematical derivations. As a consequence, simple expressions could be obtained for various output noises and noise conversion factors. It is this simplicity that makes the model a suitable means, if more complex synchronization schemes (mutually coupled or (sub) harmonically synchronized oscillators, e.g.) shall be analyzed. Moreover, the model adequately describes the output noise of synchronized oscillators with Gunn elements. It could be extended to account for upconversion and downconversion effects as well as for an RF-amplitude-dependent intrinsic noise source.

## References

[1] K. Kurokawa, "Noise in synchronized oscillators," *IEEE Trans. Microwave Theory Tech.*, vol. MTT-16, pp. 234–240, 1968.
[2] ——, "Injection locking of microwave solid-state oscillators," *Proc. IEEE*, vol. 61, pp. 1386–1410, 1973.
[3] M. E. Hines, "Large-signal noise, frequency conversion, and parametric instabilities in IMPATT diode networks," *Proc. IEEE*, vol. 60, pp. 1534–1548, 1972.
[4] J. L. Fikart and P. A. Goud, "A theory of oscillator noise and its application to IMPATT diodes," *J. Appl. Phys.*, vol. 44, pp. 2284–2296, 1973.
[5] J. J. Goedbloed and M. T. Vlaardingerbroek, "Noise in IMPATT diode oscillators at large signal levels," *IEEE Trans. Electron Devices*, vol. ED-21, pp. 342–351, 1974.
[6] ——, "Theory of noise and transfer properties of IMPATT diode amplifiers," *IEEE Trans. Microwave Theory Tech.*, vol. MTT-25, pp. 324–332, 1977.
[7] W. Freude, "Measurement of the statistics of a Gunn oscillator signal and comparison with a mathematical model," *Electron. Commun.*, vol. 30, pp. 209–218, 1976.
[8] L. Gustafsson, G. H. B. Hansson, and K. I. Lundstroem, "On the use of describing functions in the study of nonlinear active microwave circuits," *IEEE Trans. Microwave Theory Tech.*, vol. MTT-20, pp. 402–409, 1972.
[9] M. E. Hines, "Negative-resistance diode power amplification," *IEEE Trans. Electron Devices*, vol. ED-17, pp. 1–8, 1970.
[10] P. Penfield, Jr., "Circuit theory of periodically driven nonlinear systems," *Proc. IEEE*, vol. 54, pp. 266–280, 1966.

# Microwave Characterization of Silicon BARITT Diodes Under Large-Signal Conditions

GARY K. MONTRESS, MEMBER, IEEE, AND MADHU SUDAN GUPTA, SENIOR MEMBER, IEEE

***Abstract*—Experimental measurements of the small- and large-signal admittance of a silicon BARITT diode are reported. The structural characteristics of the devices are also reported, so that the results provide a basis for evaluating the large-signal analyses of BARITT diodes. A lumped-element frequency-independent equivalent circuit is proposed to represent the terminal characteristics of the device over a broad-frequency range, and is verified by comparison with the measured admittances. Simple approximations are given to describe the dependence of the device admittance on the three operating point parameters: dc bias current, signal frequency, and RF signal level.**

## I. Introduction

OF THE VARIOUS two-terminal, active, microwave semiconductor diodes (e.g., IMPATT, TRAPATT, and Gunn devices), BARITT diodes are known to have the limitations of comparatively small power output, efficiency, bandwidth, and maximum usable frequency, but they also have the advantages of lower noise and simpler technology. One of the principal characteristics of interest is the large-signal admittance $Y_D$ of BARITT diodes, which dictates the design of circuits employing the diodes, as well as determines the power and frequency limitations of the device. This admittance, defined at the terminals of the semiconductor chip (i.e., excluding the effect of parasitics introduced by the diode package), is dependent on three sets of parameters, specifying 1) the semiconductor material properties, 2) the diode doping and dimensions, and 3) the operating conditions, including the dc bias current $I_{dc}$, the temperature $T$, the signal frequency $f$, and RF voltage amplitude $V_{RF}$ of (an assumed) sinusoidal terminal voltage. In this paper, only the functional relationship $Y_D$ ($I_{dc}$, $f$, $V_{RF}$) is studied for a given diode at a given (room) temperature, i.e., with all other parameters fixed.

Large-signal operating characteristics of BARITT diodes have been theoretically studied by a number of authors in the past, both analytically and numerically [1]–[10], and the number of small-signal analyses pub-

Manuscript received May 22, 1978; revised December 1, 1978. This work was supported by the Joint Services Electronics Program.

G. K. Montress was with the Department of Electrical Engineering of the Massachusetts Institute of Technology, Cambridge. He is now with the United Technologies Research Center, East Hartford, CT 06108.

M. S. Gupta is with the Department of Electrical Engineering and Computer Science, and the Research Laboratory of Electronics, Massachusetts Institute of Technology, Cambridge, MA 02139.

0018-9480/79/0500-0458$00.75 ©1979 IEEE

lished in the literature is even larger. The various large-signal analyses differ from each other primarily in assumptions made in modeling the carrier transport in the injection and potential-barrier regions of the device. Their results, although qualitatively similar, have significant quantitative differences, making an experimental verification important.

By contrast, the experimental measurements of large-signal characteristics of BARITT devices reported in the literature are very few [11]. Other reported measurements usually include only the RF power output and dc-to-RF conversion efficiency variation with the operating point from which the device conductance can be calculated [12]. A more detailed microwave characterization of the large-signal characteristics for BARITT devices, through admittance measurements, is given here along with the details of the design of the devices used.

The purpose of this paper is threefold. First, it presents the results of the microwave measurements of the large-signal admittance of silicon BARITT diodes at the terminals of the semiconductor chip (i.e., excluding the packaging parasitics), as a function of the operating-point parameters. Such results are useful for evaluating the accuracy of theoretical analyses of large-signal operation. Second, this paper suggests simple approximations for describing the dependence of large-signal admittance on the three operating point parameters: $I_{dc}$, $f$, and $V_{RF}$. These are useful for constructing simple models for describing the characteristics of various BARITT-diode circuits, such as modulation, bandwidth, injection locking, gain compression, and saturation. Third, this paper proposes and verifies an equivalent circuit with frequency-independent lumped circuit elements to represent the device admittance over the entire range for which the BARITT diodes are an active device. Such equivalent circuits are useful because they describe the terminal characteristics of the device in terms of a small set of numbers rather than as graphical or tabulated data. They are also useful as a convenient representation of the device in computer-aided design of circuits using the device.

Two frequency-independent circuit models have been suggested for BARITT diodes in the past [13], [14]. Both of these models are theoretically derived, and neither one has been experimentally verified. The model proposed here is considerably simpler than that of [13] and more accurate than that of [14]. In addition, experimental measurements are used to establish its applicability and illustrate the determination and typical values of model parameters.

## II. The Device and the Measurements

### A. The BARITT Devices

The BARITT devices under study are M-n-$p^+$ silicon diodes with a uniformly doped drift (n) region. They consist of a 75-$\mu$m thick p-type substrate layer of 0.003-$\Omega\cdot$cm resistivity, a 10-$\mu$m thick n-type epitaxial layer of 4-$\Omega\cdot$cm resistivity, and a 0.25-mm diameter aluminum Schottky barrier formed by evaporation and annealing. The devices are mesa-isolated by etching, passivated at

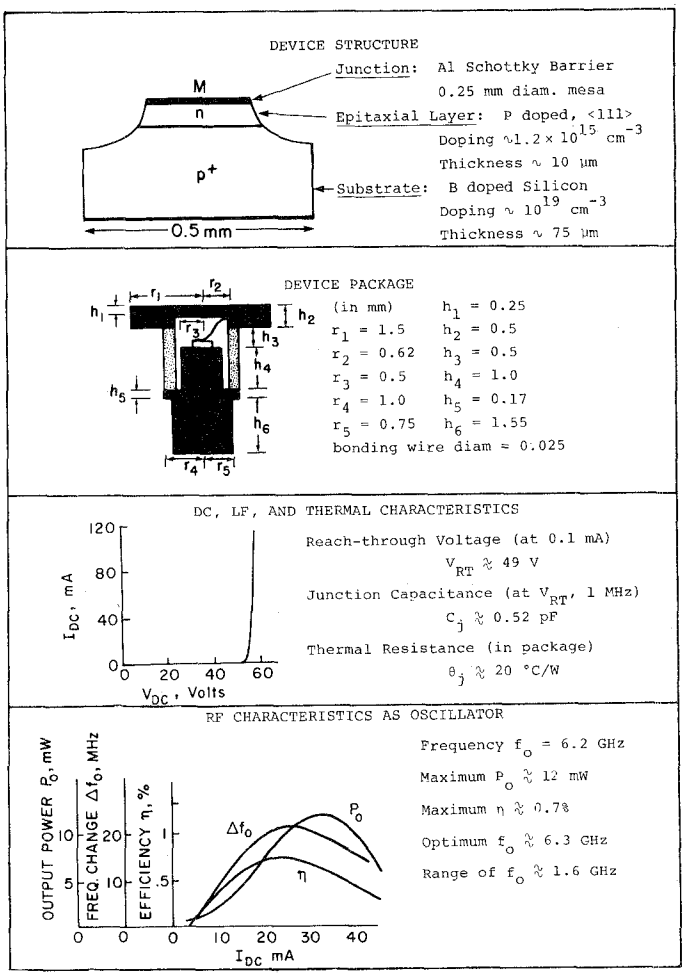


Fig. 1. Structural details of the packaged BARITT diodes and their typical operating characteristics.

the exposed silicon surfaces, mounted in the standard "pill-type" microwave packages, ultrasonically bonded by a gold wire, coated with a silicone resin, and hermetically sealed. Fig. 1 summarizes the relevant features of device and package structure, as well as the significant dc and RF characteristics. The dc $I$–$V$ characteristics are measured under nonoscillating conditions and with pulsed biasing; under dc bias conditions, the maximum safe bias current is approximately 50 mA. The RF measurements are taken in a coaxial cavity, tunable by means of movable slugs, with the diode mounted at one end, and at room temperature.

### B. Measurement of Device Admittance

The admittance of the packaged BARITT devices was measured over the frequency range 4–8 GHz (encompassing the frequency range in which the devices are active) by the usual slotted-line method, but with the following five modifications [15]. 1) The sensitivity of measurement was enhanced by superheterodyne detection at the sliding probe [15, p. 268], both in order to measure VSWR as large as 100 and to be able to use very low signal levels for small-signal measurements. 2) The power output $P_{in}$ of the signal source was monitored in order to calculate the magnitude of the RF voltage at the terminals of the diode

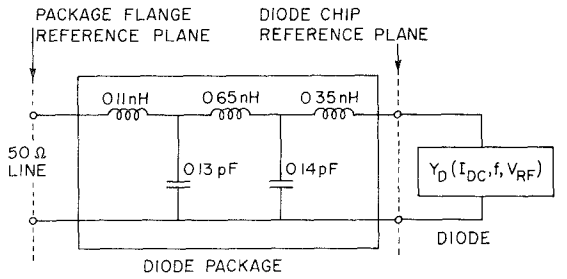


Fig. 2. Lumped equivalent circuit representation for the diode package, determined by broad-band microwave admittance measurements on open- and short-circuit packages, and used for deembedding the diode-chip admittance.

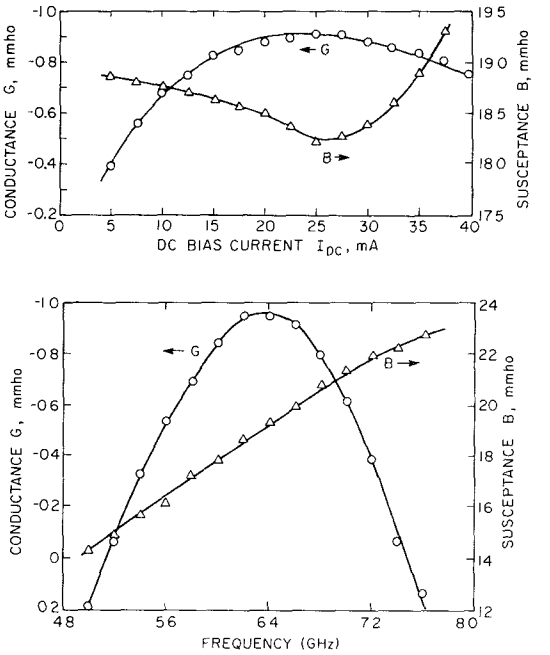


Fig. 3. Experimentally measured and deembedded small-signal admittance of the BARITT diode chip. (a) At a frequency of 6.1 GHz. (b) At a bias current of 25 mA.

chip for large-signal measurements. 3) The spectrum of the signal reflected from the device was monitored to make sure that the harmonic level is negligible. 4) The magnitude of the VSWR was found by the intermediate value method to improve the accuracy of the high measured values of VSWR [15, p. 266]. In this method the VSWR is determined from the separation $x_0$ between two points at which the detected signal is a factor (say 10) larger than that at the minimum. 5) The sign of the VSWR was established by comparing the sharpness of the minimum at two successive minima of the standing-wave pattern along the slotted line. If the device is active, the magnitude of the real part of the impedance looking towards the device is lower at a farther minimum due to the attenuation along the line; as a result the minimum is sharper, and, therefore, $x_0$ is smaller. Conversely, for a passive device, $x_0$ is larger at a minimum which is farther from the device.

The large-signal admittance $Y_D(I_{dc}, f, V_{RF})$ of the device chip, as a function of RF signal frequency and voltage, was determined from the measured admittance $Y_m(I_{dc}, f, P_{in})$ of the packaged device as follows. 1) The package was characterized by an equivalent circuit consisting of the five-element $L$–$C$ low-pass ladder network shown in Fig. 2. 2) The values of the five lumped elements were determined to fit the measured admittances of short- and open-circuited packages over 1–12 GHz [16]. 3) $Y_D$ was calculated from $Y_m$ by the usual de-embedding procedure using the above equivalent circuit [17]. 4) The amplitude of the RF voltage developed across the device was calculated from a knowledge of $Y_D$ and the signal power $P_{in}$ incident on the diode, after accounting for power losses in slotted-line and biasing-T. 5) $Y_D$ at any desired $V_{RF}$ was determined by interpolating between the de-embedded values of $Y_D$ found in step 3) for the several calculated RF voltages found in step 4).

## III. Small-Signal Characterization

### A. Small-Signal Admittance of the Device

It is found that for $V_{RF} \lesssim 0.5$ V, the measured device admittance may be called the small-signal admittance, because it is independent of $V_{RF}$, and also the application of an RF signal of this amplitude causes no observable change in $I_{dc}$. The measured small-signal admittance $Y_{D,ss}(I_{dc}, f)$ of the BARITT diode is shown as a function of bias current in Fig. 3(a), and as a function of frequency in Fig. 3(b). The experimental results are in qualitative agreement with those expected from small-signal analyses [18], while a more detailed agreement depends upon the choice of such theoretical parameters as the location of the potential minimum which are not independently evaluated in measurements. The negative conductance of the device shows a broad maximum with respect to both bias current and frequency; the susceptance is relatively insensitive to bias current and linearly related to frequency.

### B. Small-Signal Equivalent Circuit

The frequency dependence of $Y_{D,ss}$ is conveniently summarized by an equivalent circuit. A frequency-independent lumped-element equivalent circuit representation for BARITT diodes can be found by the following simple intuitive arguments. In equivalent circuit terms, the device admittance can be viewed as being composed of an active part and a parasitic part. The active part denotes a transit-time induced negative conductance, and the magnitude of negative conductance will be reduced for transit angles above or below the optimum; such a behavior is shown by a series $G_1L_1C_1$ network with a negative $G_1$. The parasitic part of the diode admittance is caused in part by the depletion-region capacitance of the punchthrough structure, represented by a capacitor $C_2$, and in part by the finite loss in the diode represented by a conductance $G_2$. This leads to the five-element lumped equivalent circuit shown in Fig. 4(a), and referred to as EQ5 below.

Given the measured (or otherwise obtained) device admittance data $Y_D(f)$ over a frequency band, the equivalent circuit elements can be found by fitting the circuit

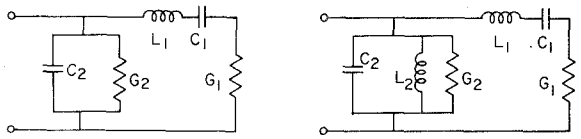


Fig. 4. Equivalent-circuit representations with frequency-independent lumped elements for the small-signal admittance of the BARITT diode chip. (a) Five-element circuit model EQ5. (b) Six-element circuit model EQ6.

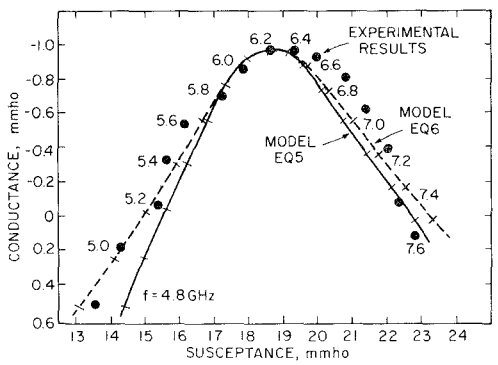


Fig. 5. A comparison of the measured small-signal admittance $Y_{D,ss}$, and the driving point admittance of the five- and six-element equivalent-circuit models for unpackaged BARITT devices. $Y_{D,ss}$ is plotted for 25 mA. For model EQ5, the element values are $G_1 = -3.3$ μmho, $L_1 = 13$ nH, $C_1 = 0.05$ pF, $G_2 = 2.3$ μmho, and $C_2 = 0.48$ pF. For model EQ6, the element values $G_1$, $L_1$, $C_1$, and $G_2$ are the same as for EQ5, while $C_2 = 0.61$ pF, and $L_2 = 4.8$ nH.

model to the data (i.e., by determining numerical values of the circuit elements so as to obtain the best match between the driving-point admittance $Y_{dr}(f)$ of the equivalent circuit, and the given device admittance $Y_D(f)$ over the frequency range of interest). A comparison of $Y_D$, and $Y_{dr}$ fitted to it, is illustrated in Fig. 5. In this figure, $Y_D$ is the measured small-signal admittance of the BARITT diode for a dc bias current of 25 mA, while $Y_{dr}$ is the admittance of EQ5 for $G_1 = -3.3$ μmho, $L_1 = 13$ nH, $C_1 = 0.05$ pF, $G_2 = 2.3$ μmho, and $C_2 = 0.48$ pF. The fitted values of $G_2$ and $C_2$ are not far from the low-frequency device conductance (at the same bias current) and depletion-region capacitance shown in Fig. 1. In general, the element values obtained by fitting will depend somewhat on the frequency range over which the fitting is carried out, as well as on the criterion of "match" between $Y_{dr}$ and $Y_D$. The five element values listed above were selected for best fit over the frequency band 4.8–7.6 GHz, and the "best fit" is defined as one minimizing the weighted mean-square difference $W(G_{dr} - G_D)^2 + (B_{dr} - B_D)^2$, summed over the set of frequencies, with a very large weight $W = 10^6$, to reflect the greater importance of device conductance in actual practice.

### C. Other Circuit Models

The circuit EQ5 is topologically similar to the circuit model for the BARITT diode proposed by Okazaki *et al.* [13], but has the conductance $G_2$ in place of an inductance in their model. Attempts to fit their model to the same experimental admittance data of Fig. 5 shows that EQ5 is superior to their model in [13]. One of the principal reasons for this superior match is that the bandwidth over which the circuit model is active is infinite for the model of Okazaki *et al.*, but finite for EQ5.

The comparison of the driving-point admittance of EQ5 and the measured $Y_{D,ss}$ in Fig. 5 shows that the difference between them is due primarily to a smaller variation of the susceptance with frequency for the circuit model. The accuracy of modeling can be significantly improved by adding an inductance $L_2$ to the equivalent circuit, which contributes to a larger frequency dependence of susceptance. This leads to the model EQ6 of Fig. 4(b), with six lumped elements. The equivalent circuit EQ6 may be viewed as a combination of EQ5 and the equivalent circuit model proposed in [13]. The fitted element values of EQ6 and the corresponding driving-point admittance are also shown in Fig. 5, with the fitting carried out over the same frequency range and with the same criterion as for EQ5.

## IV. Large-Signal Characterization

Representative results of the measured and deembedded large-signal admittance $Y_D(I_{dc}, f, V_{RF})$ for the unpackaged BARITT diode are summarized in Fig. 6. Fig. 6(a) shows the RF voltage dependence of the diode conductance $G_D$, and susceptance $B_D$. In general, this dependence is approximated very well by expressing $G_D$ and $B_D$ as a quadratic and a linear function of $V_{RF}$, respectively. For example,

$$G_D = (-0.95 + 0.075\ V_{RF}^2)\ \mu\text{mho}$$

and

$$B_D = (18.6 + 0.1\ V_{RF})\ \mu\text{mho}$$

are excellent approximations for the device admittance at 25 mA and 6.2 GHz, plotted in Fig. 6(a), where $V_{RF}$ is expressed in volts.

Fig. 6(b) shows the frequency dependence of the large-signal admittance $Y_D$ for fixed values of the RF signal voltage $V_{RF}$. The nature of this dependence is very similar to that for the small-signal admittance $Y_{D,ss}$; as a result, $Y_D$ for a given value of $V_{RF}$ can be approximated by an equivalent-circuit model, such as EQ6 with appropriately selected element values. This modeling, and the resulting dependence of the element values on RF signal voltage, are described in detail elsewhere [19].

Finally, Fig. 6(c) shows a representative example of the dependence of $Y_D$ on $I_{dc}$. As a first-order approximation, the large-signal susceptance $B_D$ is nearly independent of bias current, while the large-signal conductance has a broad maximum with respect to bias current, in a manner similar to the small-signal conductance. This is also to be expected from the equivalent circuit model, because the bias current influences only the active part ($G_1 L_1 C_1$) of the device admittance, and the device susceptance is mostly due to the parasitic part ($C_2$).

## V. Summary

The nature of the measured small- and large-signal admittances of the BARITT diode, and their dependence

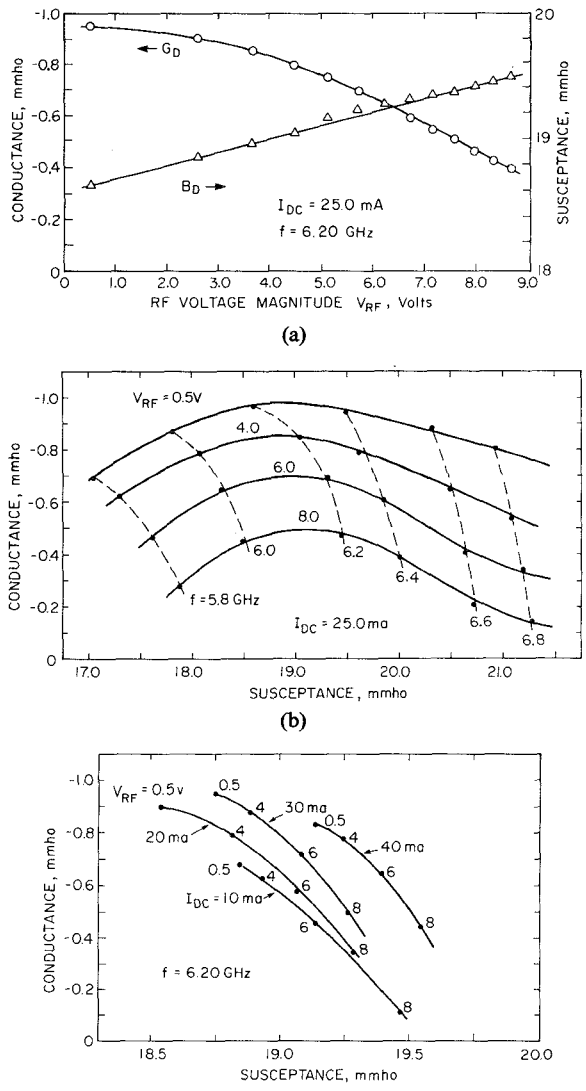


Fig. 6. Representative plots of experimentally measured and deembedded large-signal admittance $Y_D(I_{dc}, f, V_{RF})$ of the unpackaged BARITT devices. (a) Dependence on $V_{RF}$, for $I_{dc}=25$ mA, and $f=6.2$ GHz. (b) Dependence on $f$ for $I_{dc}=25$ mA. (c) Dependence on $I_{dc}$ for $f=6.2$ GHz.

upon the operating point parameters, are in agreement with the predictions of theoretical analyses. The results will serve as a basis for quantitative evaluation of large-signal analyses. The driving-point admittance of the proposed equivalent circuit model is seen to be in good agreement with the measured small-signal BARITT-diode admittance. The same model can be fitted to the large-signal admittance for a specified bias current and RF voltage amplitude, and succinctly describes the frequency dependence of the device admittance $Y_D$. The RF voltage and dc bias current dependence of $Y_D$ is well modeled by treating the conductance as a parabolic function of both $V_{RF}$ and $I_{dc}$, and the susceptance as a linear function of $V_{RF}$, but independent of $I_{dc}$. Such approximations are useful in describing the microwave-operating characteristics of BARITT diode circuits.

## References

[1] H. W. Ruegg, "A proposed punch-through, microwave negative-resistance diode," *IEEE Trans. Electron Devices*, vol. ED-15, pp. 577–585, Aug. 1968.

[2] U. B. Sheorey, I. Lundstrom, and E. A. Ash, "Analysis of punch-through-injection for a transit-time negative resistance diode," *Int. J. Electron.*, vol. 30, pp. 19–32, Jan. 1971.

[3] W. Harth and M. Claassen, "Microwave BARITT diodes, part I: Large-signal performance," *Nachrichtentech. Z.*, vol. 26, pp. 26–29, Jan. 1973.

[4] K. Kawarada and Y. Mizushima, "Large-signal analysis on negative-resistance diode due to punch-through-injection and transit-time effect," *Japan J. Appl. Phys.*, vol. 12, pp. 423–433, Mar. 1973.

[5] M. Matsumura, "Large-signal analysis of silicon BARITT diodes," *NEC Res. Development*, no. 32, pp. 1–11, Jan. 1974.

[6] J. A. C. Stewart, "BARITT-diode large-signal performance," *Electron. Lett.*, vol. 10, pp. 193–194, May 16, 1974.

[7] A. S. Tager, V. B. Sulimov, and A. K. Balyko, "The nonlinear characteristics and efficiency of injection-drift diodes," *Radio Eng. Electron. Phys.*, vol. 19(5), pp. 111–119, May 1974.

[8] G. T. Wright, "A simplified theory of the BARITT silicon microwave diode," *Solid-State Electron.*, vol. 19, pp. 615–623, July 1976.

[9] M. Karasek, "Large-signal analysis of the silicon pnp-BARITT diode," *Solid-State Electron.*, vol. 19, pp. 625–631, July 1976.

[10] S. P. Kwok and G. I. Haddad, "Power limitations in BARITT devices," *Solid-State Electron.*, vol. 19, pp. 795–807, Sept. 1976.

[11] C. P. Snapp and P. Weissglass, "On the microwave activity of punchthrough injection transit-time structures," *IEEE Trans. Electron Devices*, vol. ED-19, pp. 1109–1118, Oct. 1972.

[12] K. Okazaki, N. S. Chang, and Y. Matsuo, "Experimental studies on large-signal operation of BARITT-diode amplifiers," *Electron. Commun. Japan*, vol. 58-B, pp. 75–82, May 1975.

[13] N. Quang, "A lumped-distributed small-signal model for a class of transit-time semiconductor devices," *Int. J. Circuit Theory Appl.*, vol. 4, pp. 357–370, Oct. 1976.

[14] K. Okazaki, N. S. Chang, and Y. Matsuo, "A frequency-independent large-signal equivalent circuit for a BARITT diode and its application to an amplifier," *IEEE Trans. Microwave Theory Tech.* vol. MTT-24, pp. 527–529, Aug. 1976.

[15] E. L. Ginzton, *Microwave Measurements*. New York: McGraw-Hill, 1957, ch. 5.

[16] I. W. Pence, Jr., and P. J. Khan, "New broad-band equivalent circuit determination for Gunn diodes," *IEEE Trans. Microwave Theory Tech.*, vol. MTT-18, pp. 784–789, Nov. 1970.

[17] R. F. Bauer and P. Penfield, Jr., "De-embedding and unterminating," *IEEE Trans. Microwave Theory Tech.*, vol. MTT-22, pp. 282–288, Mar. 1974.

[18] D. J. Coleman, "Transit-time oscillations in BARITT diodes," *J. Appl. Phys.*, vol. 43, pp. 1812–1818, Apr. 1972.

[19] G. K. Montress, "Fabrication and large-signal characterization of BARITT diodes," Ph.D. dissertation, Massachusetts Institute of Technology, Cambridge, 1976.